DOI: 10.13009/EUCASS2023-533
Aerospace Europe Conference 2023 – 10TH EUCASS – 9TH CEAS

Investigation of fluid-structure interaction on a flexible cantilevered panel due to shock impingement

Kartika Ahuja[*†] and Srisha Rao MV*[*]*
** Indian Institute of Science*
Bengaluru, India
kartikaahuja@iisc.ac.in
[†] Corresponding Author

Abstract

This study investigates the effect of shock impingement at Mach 6.5 flow on a thin compliant panel. A wedge of a 24.7 degree angle generates a shock wave that impinges on a thin cantilevered panel. This interaction of the shock with the panel produces flow-induced vibrations and aeroelastic coupling between the panel and the flow field. Experiments were conducted on a rigid plate, and a compliant panel, and the results were compared. The compliant panel shows a reduction in the size of the separation bubble. Numerical simulations were performed to gain a comprehensive understanding of the mechanisms underlying aeroelastic coupling.

1. Introduction

Interactions between shock waves and boundary layers are well-studied [1,2]. Research on Shock Boundary Layer Interactions (SBLI) focuses mostly on rigid structures with interactions produced by impinging oblique shocks and compression ramps. Several components, including vehicle control surfaces and complicated geometric features, can generate shocks. The shock-induced unsteady loadings adversely impact the performance of the vehicle. Structures with low stiffness are required for lightweight vehicles in hypersonic flows. So, structures are more vulnerable to aeroelastic instability and fluid-structure interactions. When SBLI is present, it becomes more challenging to study fluid-structure interactions. There needs to be an understanding of how shock boundary layer interactions affect a compliant panel's flow field and structural modes. Improving the accuracy of aeroelastic modelling tools used in designing a hypersonic aircraft requires a detailed characterisation of fluid-structure coupling.

Shockwave boundary layer interactions on flexible panels have not been studied much until recently. Spottswood et al. [3] conducted preliminary experiments with a shock impinging on a compliant panel at Mach 2. Willems et al. [4] conducted an experiment in which a shock impinged on a clamped, compliant panel at Mach numbers between 2.5 and 4.5. Daub et al.[5] conducted similar experiments in Mach flows of 3 and 4 using a fast-moving shock sweeping across an elastic surface to analyse the oscillations of the elastic panel generated by the flow field and vice versa. It was demonstrated that the elastic panel might affect the flow field topology and behaviour in the separated zone both statically and dynamically. The interaction between surface deformation and shock-induced separation on a panel in supersonic flow was also studied computationally by Brouwer et al.[6]. They found that the mean size of the shock-induced separation bubble might significantly increase and decrease as a result of static surface deformations.

Extensive work has been performed to study flow-induced vibrations caused by shock impingement on fully clamped panels. Currently, data from the cantilevered flat panel undergoing fluid-structure interaction because of shock impingement is very limited. Moreover, most experiments involving compliant panels were limited to supersonic Mach numbers. In contrast, this work aims to investigate the response of a cantilevered compliant panel and to study the fluid-structure interactions caused by shock impingement at Mach 6.5. It is critical to comprehend how the panel's response changes in the presence of SBLI and how the panel deflection, in turn, affects the flow field and separation bubble dynamics. The effect on the response of the compliant panel due to shock impingement is reported by the author in previous studies[7]. This work investigates the effect of the compliant panel on the flow field. Fluid-structure interactions along with SBLI dictate the dynamics of the separation bubble as it interacts with the compliant panel. Numerical simulations were also performed on a cantilevered panel in hypersonic flow using ANSYS coupling with impinging shock. The separation bubble size was compared with a rigid case to see how the compliant panel affects the flow field. The remainder of the paper is organised as follows: Section 2 describes the test facility, model design, and Numerical simulation details employed in the study are given in Section 3, whereas Section 4 reviews the results for shock impingement on the rigid plate and a compliant panel, and the conclusions and further improvements are provided in Section 5.

DOI: 10.13009/EUCASS2023-533

2. Experimental Facility

Experiments were conducted in the Hypersonic Shock tunnel (HST 2) facility at the Indian Institute of Science, Bengaluru. Hypersonic shock tunnel 2 is a conventional shock tunnel with a driven section, driver section, nozzle, dump tank, and high vacuum system. The driver and driven sections of the HST 2 facility were combined to create a Ludwieg tube. The flow expands through the nozzle and test section due to an unstable expansion wave created when the valve opens. Figure 1 depicts a schematic of the Experimental facility. The facility generates a Mach 6.5 flow with Reynolds numbers ranging from 9 to 33 million/m. Table 1 shows the freestream conditions for fill pressure of 30 bar which is used in this investigation. A continuous flow of 35 ms test time is obtained. The schematic of the experimental model is presented in Figure 2. The test model consists of a rigid, oscillating part with a shock generator positioned above. A wedge of angle 24.7 degrees creates an oblique shock for Mach 6.5 flow. The predicted inviscid impingement length location is 140 mm, calculated using oblique shock relations. The rigid part is 100 mm long, 20 mm thick, and 90 mm wide. It has a leading-edge angle of 45 degrees. The oscillating panel is clamped to the rigid plate using countersunk screws. Further details of the experimental facility and the model are given by the author in previous studies [7]. The entire model is made from aluminium. Figure 2(a) shows the test model and the arrangement of fixing the oscillating panel to the rigid part. Table 2 shows the details of the oscillating panel.

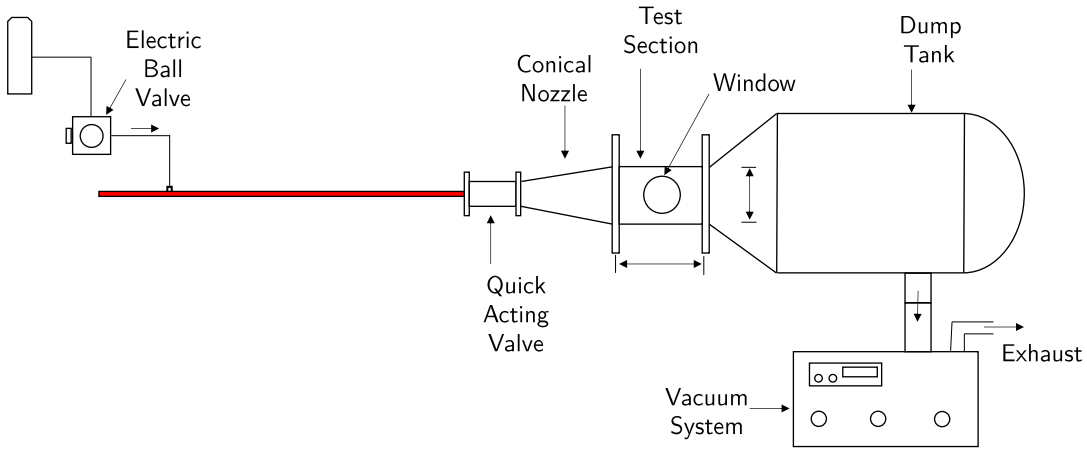

Figure 1: Schematic of HST 2 facility

Table 1: Free Stream Conditions

Mach Number	$P_\infty (Pa)$	T_∞(K)	ρ_∞	U_∞	Reynolds number (million/m)
6.61	539	30.3	0.059	741.93	24.51

Table 2: Model Properties

Length(mm)	Width(mm)	Thickness (mm)	Young's modulus (GPa)	Density(kg/m^3)
130	90	2	52.7	2668.75

All schlieren and pressure measurements have been synchronised in the present study. High-speed Schlieren imaging is a non-intrusive method for visualising flow field. In high-speed flows, a shock and an expansion fan cause sharp density changes that alter the refractive index and bend light. This creates a distortion that leads to variations in spatial intensity, which can be visualised using the Schlieren system. A standard Z-type Schlieren system, shown in Fig. 3, typically includes a light source, two plane mirrors, two concave mirrors (one for collimating and one for focusing), and a knife edge. Photron FASTCAM SA4 cameras capture images at a resolution of 320 x 240 pixels at 40 000 Hz.

DOI: 10.13009/EUCASS2023-533

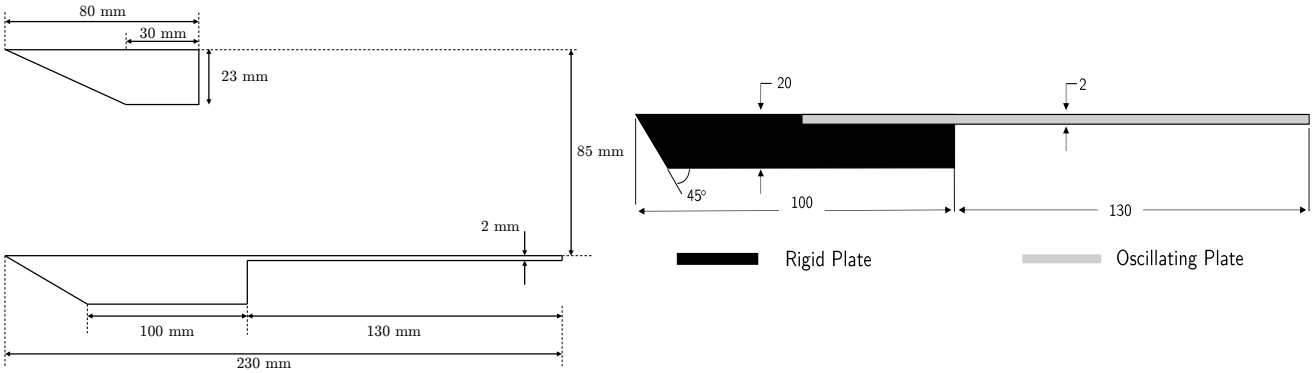

(a) (b)

Figure 2: (a) Schematic of the compliant panel with shock generator (b) Dimensions of the oscillating and rigid panel

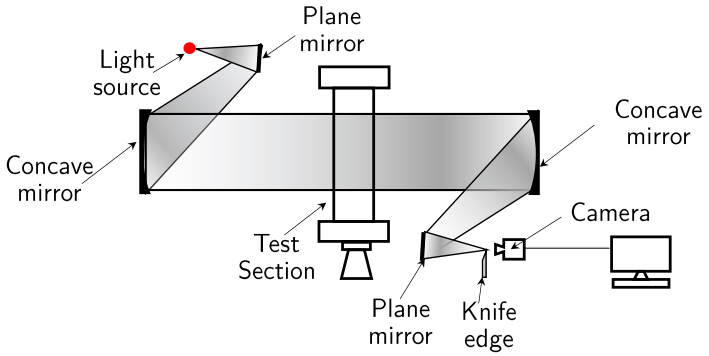

Figure 3: Schematic of Z-type schlieren.

3. Numerical Simulations

Numerical simulations were conducted to investigate the shock impingement on a rigid plate using ANSYS Fluent. The freestream conditions used in the simulation are specified in Table 1. Figure 4 (a) depicts the computational domain in the simulation. Commercial grid generating software, ICEMCFD, was utilised to generate a structured grid. A highly refined grid with 360,000 elements was employed. Figure 4 (b) displays a coarser mesh for reference. The air was modelled as calorically perfect, with viscosity and thermal conductivity determined using Sutherland's three-coefficient model. Convergence of the solution was achieved when the residuals of continuity, momentum, and energy dropped below 10^{-4}. The simulation employed a density-based implicit solver to capture the high-speed Mach 6.5 flow's behaviour accurately. High-order schemes were integrated into the solver to effectively capture the shock wave and resolve flow features near the impingement region.

Transient simulations were performed to investigate the shock impingement on the compliant panel. It provided insights on the dynamics of the separation bubble on the compliant panel by employing the coupling solver capabilities ANSYS. The ANSYS coupling solver enables the simultaneous solution of fluid dynamics and structural mechanics equations, facilitating the accurate modelling of fluid-structure interactions. The Navier-Stokes equations were solved using the finite volume method for the fluid dynamics analysis. The fluid solver is an implicit cell-centred second-order upwind solver used to produce the transient fully laminar solution. The thin compliant panel was modelled using the finite element method on the structural side. The panel's cantilevered configuration was incorporated into the simulation setup. The pressure distribution acted as a loading condition on the structural analysis, influencing the panel's deformation and vibrations. Conversely, the panel's displacement and deformation affected the surrounding flow field, resulting in aeroelastic coupling.

DOI: 10.13009/EUCASS2023-533

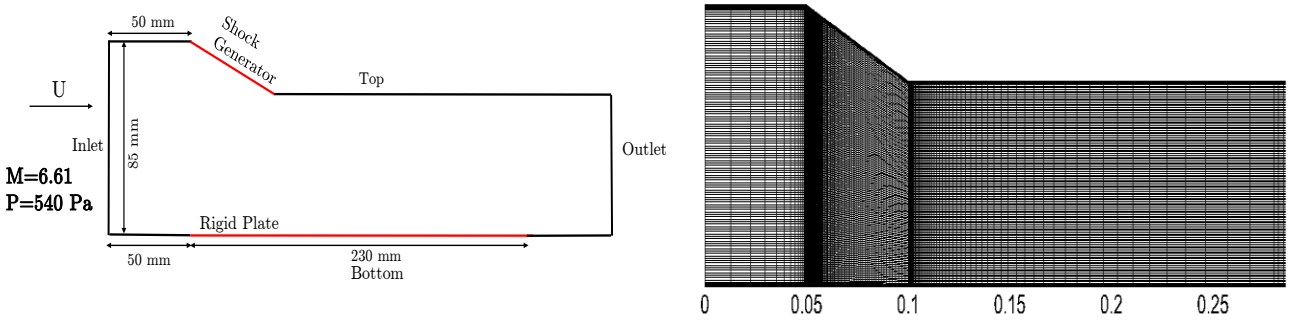

(a) (b)

Figure 4: (a) Computational domain for rigid plate (b) Coarse mesh.

The computational mesh used in the simulation for the compliant panel is shown in Figure 5. For the grid generation, a structured grid was utilised to capture the shock wave and accurately resolve the flow features near the impingement region. The grid was refined in the vicinity of the panel and the shock wave to capture the localised flow phenomena with higher accuracy. A highly refined grid with 855,000 elements was employed. An appropriate grid resolution was chosen to balance computational efficiency and solution accuracy. The grid quality was carefully evaluated to ensure a smooth and well-behaved mesh, free from distortion or irregularities that could introduce numerical errors. Regarding the boundary conditions, the inlet boundary was defined for the free stream conditions given in Table 1. A pressure boundary condition was imposed at the outlet boundary to facilitate a smooth flow exit. In the simulation, a time step of $\Delta t = 1e\text{-}4$ sec was utilised to discretise the temporal domain. This time step resolution allowed for precisely tracking the evolving flowfield and shock impingement phenomena. By employing a fine time step, the simulation captured the system's transient behaviour with high temporal accuracy, enabling a detailed analysis of the dynamic processes involved in the shock impingement on the compliant panel. The current work is ongoing, and the simulations have been conducted up to a test time of 20 ms due to the computationally intensive nature of the simulations. However, the achieved simulation results provide valuable insights into the system's behaviour during the initial 20 ms, laying the basis for further analysis and understanding of the shock impingement phenomenon.

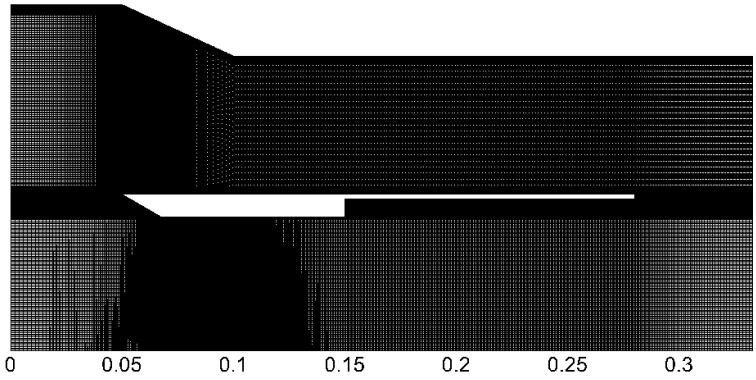

Figure 5: Computational mesh for the compliant panel case.

4. Results

4.1 Schlieren Images

Figure 6 illustrates Schlieren images depicting shock boundary layer interactions on (a) the Rigid panel and (b) the compliant panel when subjected to shock impingement. The shock generator's incident shock wave impacts the panel at inviscid impingement length of 140 mm from its leading edge. Across shock, there is an adverse pressure gradient, separating the boundary layer and forming a separation bubble. Subsequently, the shear layer reattaches downstream due to a favourable pressure gradient, giving rise to a reattachment shock. The significant flow features, including the incident shock, leading edge shock, separation shock, and reattachment shock, are highlighted in Figure 6. The red

DOI: 10.13009/EUCASS2023-533

lines in the figure denote the separation bubbles. Notably, the shock impingement induces deformation in the compliant panel, which influences the flow field and causes changes in size and location of the separation bubble.

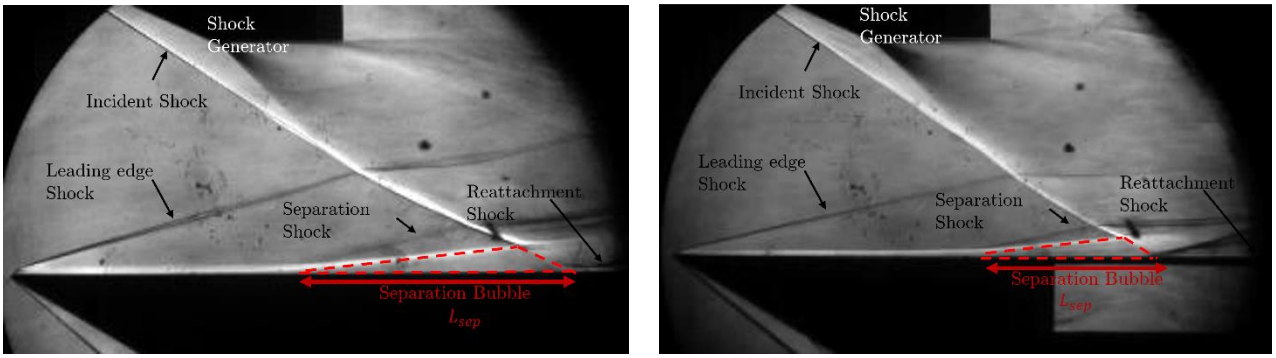

(a) (b)

Figure 6: Schlieren image showing main features when shock impinges on (a)Rigid panel and (b) Compliant panel.

In the case of the compliant panel, an intriguing observation is that the size of the separation bubble is notably diminished. The inherent flexibility of the compliant panel allows it to deform in response to the shock impingement, thereby altering the flow field dynamics. This deformation induces changes in the boundary layer and promotes a more favourable pressure gradient. Consequently, the separation bubble becomes smaller in size compared to rigid panels. This reduction in the separation bubble's dimensions is a significant finding, highlighting the role of compliance in mitigating flow separation and enhancing flow control capabilities.

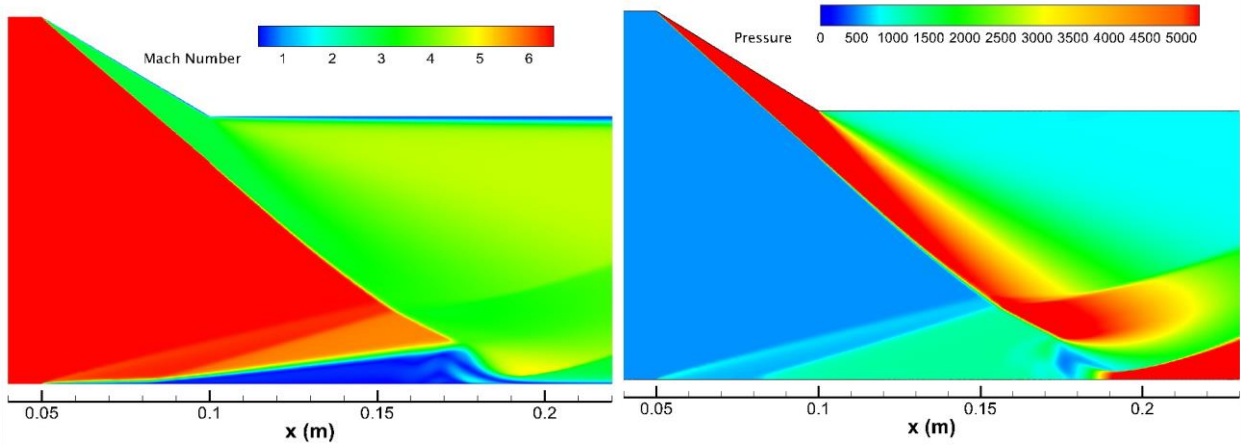

(a) (b)

Figure 7: Shock-boundary layer Interactions on the rigid plate. Contours of (a) Mach Number and (b) Pressure.

4.2 Shock Boundary layer interactions on Rigid Plate

This section shows results for the case when shock impinges on the rigid plate. Figure 7 shows the Mach number and Pressure field for shock impingement on a rigid plate simulated numerically. The Mach number contour provides insights into the flowfield distribution across the plate's surface. On the other hand, the pressure contour visualises the pressure distribution across the rigid plate due to the shock impingement. The impinging shock is the initial shock wave generated by the wedge. The leading-edge shock is also observed in the figure. Furthermore, the figure illustrates the shear layer separation and the formation of a separation bubble. The shear layer separation occurs when the boundary layer separates from the plate's surface, creating a region of flow recirculation. This is followed by forming a separation bubble, characterised by a localised area of separated flow.

DOI: 10.13009/EUCASS2023-533

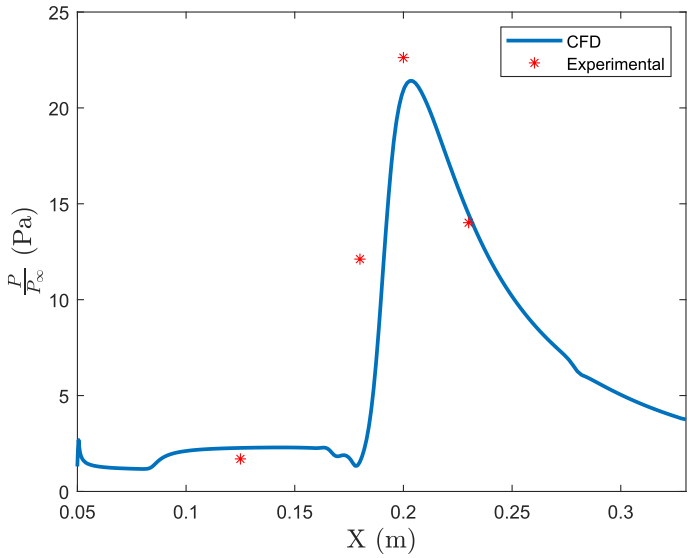

Figure 8: Pressure distribution on the wall of the rigid plate.

A comparison of the surface pressure distribution normalised by a corresponding freestream pressure on a rigid plate obtained experimentally and numerically is shown in Figure 8. Four PCB pressure sensors were flush mounted at locations of 75 mm, 130 mm, 150 mm and 180 mm from the leading edge, respectively. These sensors have a sensitivity of 100 mV/psi. Signals are recorded by a data acquisition system, NI PXI-6133, at a sampling rate of 1 Mhz. The wall pressure distribution exhibits a two-step pressure rise, depicted in Figure 7. As the shock wave interacts with the boundary layer, a separation shock is formed, leading to a significant rise in pressure. This occurs as the boundary layer separates from the wall. Following the separation shock, a plateau region appears in the pressure distribution. A uniform pressure level characterises this region. It arises as the flow transitions from the separated boundary layer to a recirculation zone. The flow remains stagnant in this region, resulting in nearly constant pressure. Subsequently, a reattachment shock is formed downstream, causing another notable rise in pressure. The reattachment shock occurs as the flow reattaches to the wall after the recirculation zone. The pressure distribution of the simulation shows good agreement with the experimental results.

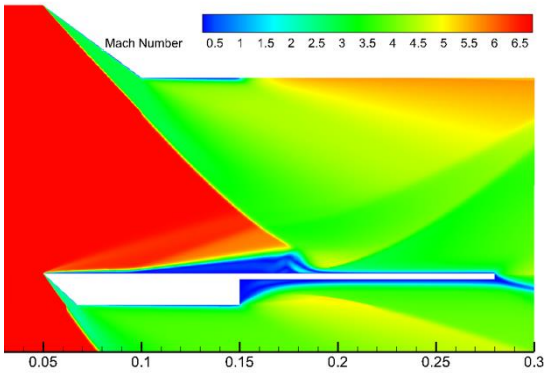

Figure 9: Contours of Mach Number on Shock impingement on Compliant panel.

4.3 Shock-Boundary layer interactions on Compliant panel

This section studies the dynamics of the separation bubble when shock impinges on a compliant panel numerically. Figure 9 shows the contours of the Mach number as shock impinges on the compliant panel. It shows all the main features, including impinging shock, leading edge shock, separation shock shear layer and reattachment shock. Figure 10 shows the flow field at various time instants of (a) 0 ms, (b) 2.1 ms, (c) 3.7 ms, (d) 5.6 ms, (e) 8.2 ms and (f) 10 .8 ms, respectively. The compliant panel is at zero deflection at the start of the test time at zero ms. However, as shock imposes pressure, the plate starts deflecting, as shown in time instants of 2.1 ms and 3.7 ms, with 5.6 ms corresponding to the location of maximum deflection. As the structure deflects downwards, there will be an expansion fan across

DOI: 10.13009/EUCASS2023-533

which the pressure will be reduced. The plate keeps deforming till it reaches a position where all the elastic and pressure forces are balanced. The downward aerodynamic forces attain a minimum value when reaching the lowest deflection location. Meanwhile, upward elastic restoring forces generated by the plate continues to increase during the process and attain a maximum value greater than the aerodynamic force at the lowest deflection location. Consequently, the resultant force causes the plate to move upward. After that, it starts returning, and 10.8 ms corresponds to the return to the initial position and the end of one cycle.

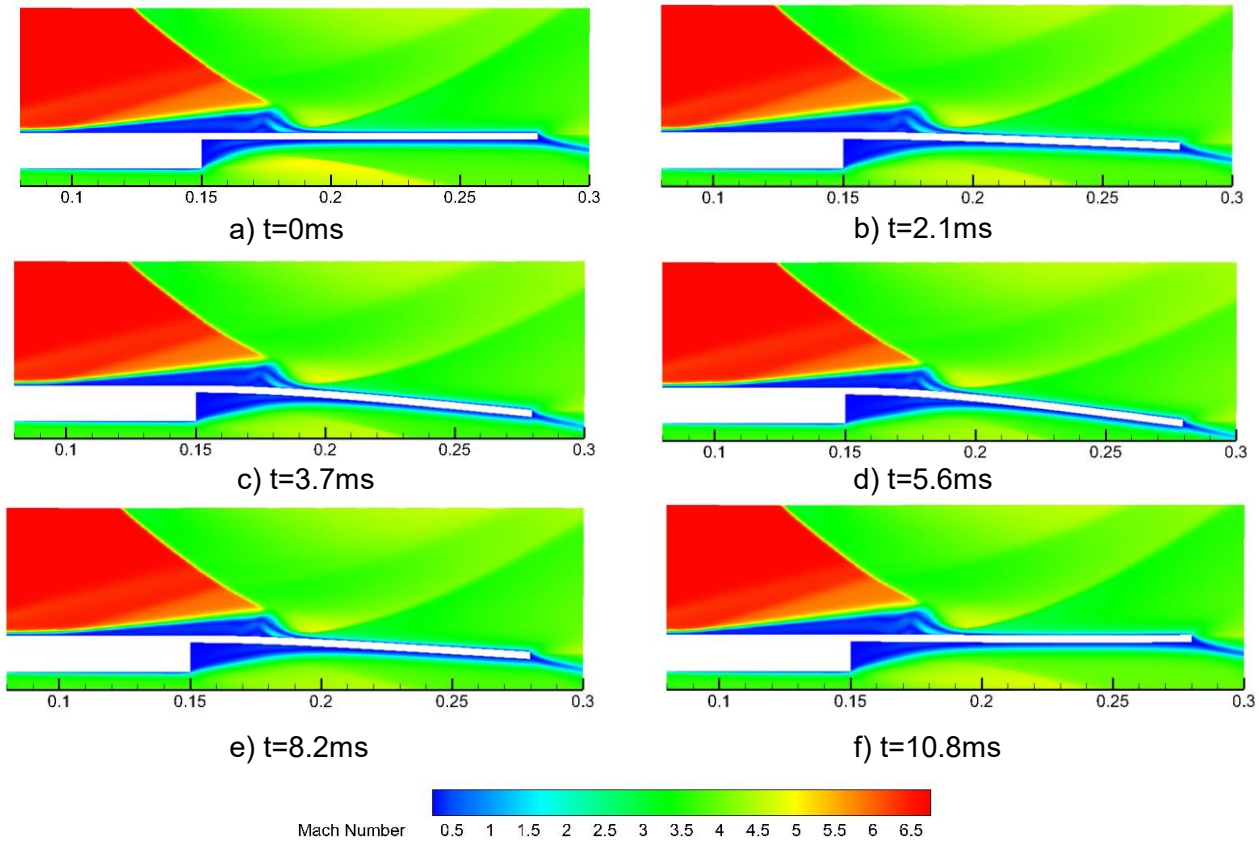

Figure 10: Mach number contours at time instants (a) 0 ms (b) 2.1 ms (c) 3.7 ms (d) 5.6 ms (e) 8.2 ms and (f) 10 .8 ms, respectively, showing the deformation of the compliant panel and downstream movement of the separation bubble.

Figure 11 displays pressure signals as a function of time for a duration of 20 ms at 75 mm and 100 mm locations from the leading edge of the compliant panel. The pressure variation over time provides insights into the dynamic behaviour of the panel and its influence on the surrounding flow field. The pressure at these specified locations exhibits distinct changes as the compliant panel undergoes deflection in response to the shock impingement. The pressure signal captures the transient nature of the flow-structure interaction, with fluctuations corresponding to the panel's deformation. Notably, the minimum pressure corresponds to the maximum deflection position in the compliant panel. When the panel deflects, it creates an expansion fan, leading to decreased pressure. This decrease in pressure aligns with the moment the panel experiences its maximum displacement. The panel's deflection alters the local flow dynamics, resulting in pressure variations that can be observed in the pressure signals. The pressure changes captured in the figure provide valuable insights into the relationship between the panel's deformation and the corresponding alterations in the flow field. This understanding is crucial for assessing the aeroelastic coupling effects, flow control mechanisms, and the overall structural response of compliant panels subjected to shock impingement scenarios.

DOI: 10.13009/EUCASS2023-533

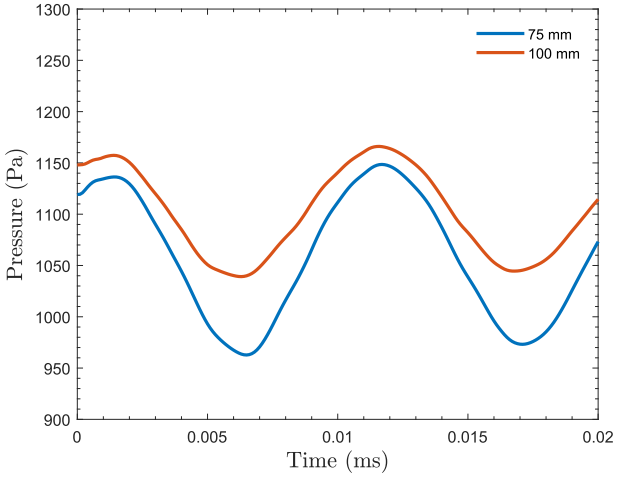

Figure 11: Pressure Signals plotted using numerical simulation at 75 mm and 100 mm locations from the leading edge on the compliant panel.

5. Conclusions

This study investigated the dynamics of the separation bubble on the compliant cantilevered panel subjected to shock impingement at Mach 6.5 experimentally and numerically. During experiments, Schlieren images show a reduction in the separation bubble size in the case of a compliant panel compared to the rigid plate. This may be attributed to the deformation of the compliant panel, which reduces the adverse pressure gradient and leads to the bubble's downstream movement. The numerical simulations were performed to gain insights into the bubble dynamics. The pressure on the rigid wall is plotted for experiments and numerical simulations and is in good agreement. Mach number contours and Pressure field are shown for the rigid plate subjected to shock impingement. Pressure on the compliant panel is found to be varying with the deformation of the plate with the same frequency as that of the plate. The Mach number contours for the panel deformation are shown at various instants to show how the deflection of the plate impacts the movement of the separation bubble.

References

[1] Dolling, D. S. "Fifty Years of Shock-Wave/Boundary-Layer Interaction Research: What Next?" *AIAA Journal*, Vol. 39, No. 8, 2001, pp. 1517–1531. https://doi.org/10.2514/2.1476.

[2] Délery, J., and Dussauge, J. P. "Some Physical Aspects of Shock Wave/Boundary Layer Interactions." *Shock Waves*, Vol. 19, No. 6, 2009, pp. 453–468. https://doi.org/10.1007/s00193-009-0220-z.

[3] Michael Spottswood, S., Beberniss, T. J., and Eason, T. G. Full-Field, Dynamic Pressure and Displacement Measurements of a Panel Excited by Shock Boundary-Layer Interaction. 2013.

[4] Willems, S., Gülhan, A., and Esser, B. "Shock Induced Fluid-Structure Interaction on a Flexible Wall in Supersonic Turbulent Flow." Vol. 5, 2013, pp. 285–308. https://doi.org/10.1051/eucass/201305285.

[5] Daub, D., Willems, S., and Gulhan, A. "Experiments on the Interaction of a Fast-Moving Shock with an Elastic Panel." *AIAA Journal*, Vol. 54, No. 2, 2016, pp. 670–678. https://doi.org/10.2514/1.J054233.

[6] S. B., Brouwer, K. R., Gogulapati, A., and Mcnamara, J. J. "Interplay of Surface Deformation and Shock-Induced Separation." Vol. 55, No. 12, 2017, pp. 24–27. https://doi.org/10.2514/1.J056030.

[7] Ahuja, K., and Rao, S. M. V. Response of a Cantilevered Plate to Shock Impingement in Hypersonic Flows, 2023. In 25th AIAA International Space Planes and Hypersonic Systems and Technologies Conference (p. 3072). https://doi.org/10.2514/6.2023-3072